Fixed-point distributions of short-range Ising spin glasses on hierarchical lattices

Sebastião T. O. Almeida[1,2,*] and Fernando D. Nobre[1,3,†]

[1]*Centro Brasileiro de Pesquisas Físicas, Rua Xavier Sigaud 150, 22290-180 Rio de Janeiro, RJ, Brazil*

[2]*Colégio Técnico da Universidade Federal Rural do Rio de Janeiro, Seropédica, 23891-000 Rio de Janeiro, RJ, Brazil*

[3]*National Institute of Science and Technology for Complex Systems, Rua Xavier Sigaud 150, 22290-180 Rio de Janeiro, RJ, Brazil*

(Received 18 September 2014; published 25 March 2015)

Fixed-point distributions for the couplings of Ising spin glasses with nearest-neighbor interactions on hierarchical lattices are investigated numerically. Hierarchical lattices within the Migdal-Kadanoff family with fractal dimensions in the range $2.58 \leqslant D \leqslant 7$, as well as a lattice of the Wheatstone-Bridge family with fractal dimension $D \approx 3.58$ are considered. Three initial distributions for the couplings are analyzed, namely, the Gaussian, bimodal, and uniform ones. In all cases, after a few iterations of the renormalization-group procedure, the associated probability distributions approached universal fixed shapes. For hierarchical lattices of the Migdal-Kadanoff family, the fixed-point distributions were well fitted either by stretched exponentials, or by q-Gaussian distributions; both fittings recover the expected Gaussian limit as $D \to \infty$. In the case of the Wheatstone-Bridge lattice, the best fit was found by means of a stretched-exponential distribution.

DOI: 10.1103/PhysRevE.91.032138 PACS number(s): 05.50.+q, 75.10.Nr, 75.10.Hk, 64.60.De

I. INTRODUCTION

In spite of considerable efforts carried throughout the past decades, an appropriate theoretical framework for the Ising spin glass (SG) is still lacking [1–3]. Its simple formulation in terms of binary variables has attracted many workers, which have followed several computational and analytical procedures, leading to a wide variety of results and interpretations, some of them contradictory, so that the model remains very controversial. From the analytical point of view, most approaches were carried on its mean-field formulation, defined in terms of infinite-range interactions. The appropriate mean-field solution is expressed in terms of an infinite number of order parameters, characterizing an order-parameter function, manifesting the property of replica-symmetry breaking [1–6]. Among many controversial points, an identification of those characteristics from this mean-field solution that should persist in the limit of short-range (e.g., nearest-neighbor) interactions represents one of the major questions in the Ising SG problem nowadays. Motivated by this, a lot of work has been pursued on nearest-neighbor-interaction three-dimensional Ising SG models, for which it is generally accepted nowadays that a SG phase occurs at finite temperatures [4–19]; it should be emphasized that some of this work has required extensive computational efforts.

Hierarchical lattices emerged in the context of real-space renormalization group (RG), carrying the advantage that such a technique becomes exact for pure systems defined on these lattices [20]. They are constructed through successive similar operations at each hierarchical level, e.g., at each level one replaces bonds by unit cells, like those shown in Fig. 1. The main motivation for their use concerns the fact that some of these lattices approach Bravais lattices, e.g., the hierarchical lattice defined by the cell of the Migdal-Kadanoff (MK) family [21–23] in Fig. 1(a) with $p = 4$, as well as the one defined by the cell of the Wheatstone-Bridge (WB) family in Fig. 1(b), have been both used in the literature to approach the cubic lattice [20]. It should be mentioned that the MK approach is exact only for pure one-dimensional systems [23], and due to the parallel (i.e., independent) paths joining the external sites of the unit cell of Fig. 1(a), it becomes progressively a worse approximation when applied to higher-dimension Bravais lattices. Surprisingly, in the case of short-range Ising SGs, the MK approach has provided some estimates (e.g., critical temperatures of distinct SG models, characterized by different probability distributions for the couplings, on the $D = 3$ hierarchical lattice) that are relatively close to the most recent ones from extensive numerical simulations on the corresponding Bravais lattices. However, due to the simplicity of the MK approach, these results are usually considered as mere coincidences, having no fundamental reason to yield small discrepancies from the estimates of more powerful methods. In spite of this, they have been very useful in the development of the SG theory throughout the years; some of these results will be mentioned later on.

In general, the RG may not be considered as an exact procedure for random systems on hierarchical lattices; however, it is expected to represent a good approximation on these lattices, since in many cases, pure systems appear as particular limits of random models. These lattices has been very useful for Ising SGs [7,10,11,16,24–38], mostly due to the possibility of obtaining estimates that are, in some cases, very close to those of more time-consuming techniques, by performing relatively low-time-consuming numerical computations. Some of these results concerning the lower critical dimension d_l, above which one finds a SG phase at finite temperatures, as well as critical-temperature estimates, should be mentioned. (i) The bounds for the lower critical dimension, $2 < d_l < 3$, were first obtained on MK lattices [7], a few years before their confirmation in Refs. [10,39–42] through studies of excitations from ground states; these domain-wall analyses have been improved lately [43,44], reinforcing the early conclusions. (ii) A recent combination of extensive numerical and theoretical results on Bravais lattices [45] suggested the lower critical dimension to be exactly $d_l = 5/2$, confirming the early estimate of Ref. [11] for MK lattices. (iii) The SG

*Corresponding author: stalme@cbpf.br

†fdnobre@cbpf.br

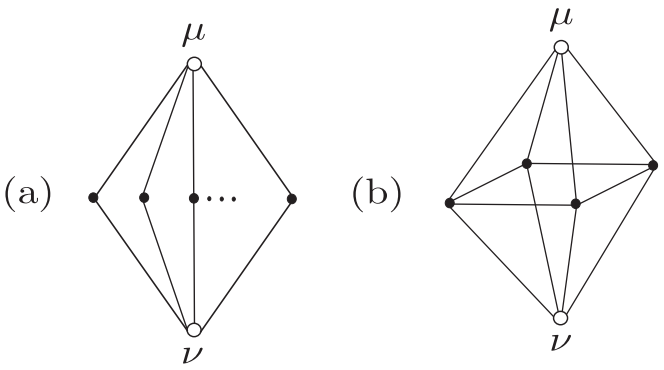

FIG. 1. Basic cells of the hierarchical lattices investigated herein, both with scaling factor $b = 2$. (a) The diamond cell belongs to the Migdal-Kadanoff family [21,22], is defined by p parallel paths, and presents a fractal dimension $D = [\ln(2p)]/\ln 2$. (b) The cell of the Wheatstone-Bridge family ($D \approx 3.58$) whose hierarchical lattice approaches the cubic lattice [20]. The empty circles (μ and ν) represent external sites of the cell, whereas the black circles are internal sites to be decimated in the RG procedure.

critical temperatures on the MK lattice of fractal dimension $D = 3$, for symmetric Gaussian and bimodal distributions [7], present relative discrepancies of about 7%, when compared with the recent estimates from Monte Carlo simulations on a cubic lattice [14]. (iv) Recently, the estimates of item (iii) were improved further through the hierarchical lattices defined by the cell of Fig. 1(b) [36], which when compared with the estimates of Ref. [14] yields a relative discrepancy of about 3% in the Gaussian case, whereas for the symmetric bimodal distribution the two estimates essentially coincide (leading to a relative discrepancy of about 0.3%). (v) Studies on a self-dual hierarchical lattice with scaling factor $b = 3$ and fractal dimension $D = 2$ led to an estimate for the stiffness exponent y [25] ($y = -1/\nu$, where ν is the exponent associated with the divergence of the correlation length at zero temperature) in agreement with those obtained from other, more time-consuming, numerical approaches on a square lattice [44,46]. An analysis of the $\pm J$ Ising SG model [33] on the same hierarchical lattice gave a ferromagnetic-paramagnetic critical frontier that represents a good approximation for the one of the corresponding model on a square lattice.

The above-mentioned results motivate us to study further properties of SGs on hierarchical lattices. As usual in the RG procedure, after each decimation step the set of coupling constants $\{J_{ij}\}$, as well as the temperature T, vary in such a way that the probability distribution $P(K_{ij})$, associated with the dimensionless ratios $\{K_{ij}\}$ [$K_{ij} = J_{ij}/(kT)$], changes its shape. At the phase transition separating the phases paramagnetic SG, the probability distribution remains unchanged, i.e., fixed. The purpose of the present work is to investigate the functional form for the fixed-point distribution of Ising SGs on the hierarchical lattices defined by the unit cells of Fig. 1. In the case of the MK family [Fig. 1(a)] we will study hierarchical lattices with fractal dimensions varying in the interval from $D \approx 2.58$ (corresponding to unit cells with $p = 3$ parallel paths), up to $D = 7$ (corresponding to unit cells with $p = 64$ parallel paths). In the next section we define the model and the numerical procedure to be used. In Sec. III we exhibit the numerical data associated with the fixed-point distributions, together with the analytical forms proposed for their fits. Finally, in Sec. IV we present our conclusions.

II. MODEL AND NUMERICAL PROCEDURE

Herein we investigate short-range Ising SGs defined by the Hamiltonian,

$$\mathcal{H} = -\sum_{\langle ij \rangle} J_{ij} S_i S_j \quad (S_i = \pm 1). \tag{1}$$

The sum $\sum_{\langle ij \rangle}$ applies to pairs of nearest-neighbor spins on the hierarchical lattices defined by the cells of Fig. 1, whereas the $\{J_{ij}\}$ represent independent random couplings acting on each pair of spins of the lattice. The couplings $\{J_{ij}\}$ will be considered as initially following three different symmetric distributions, namely, the Gaussian, bimodal, and uniform ones, defined respectively, as

$$P(J_{ij}) = \frac{1}{\sqrt{2\pi J^2}} \exp\left(-\frac{J_{ij}^2}{2J^2}\right), \tag{2}$$

$$P(J_{ij}) = \frac{1}{2}[\delta(J_{ij} - J) + \delta(J_{ij} + J)], \tag{3}$$

$$P(J_{ij}) = \begin{cases} \frac{1}{2J} & \text{if } -J \leqslant J_{ij} \leqslant J, \\ 0 & \text{(otherwise).} \end{cases} \tag{4}$$

The RG procedure works inversely to the lattice generation, i.e., through a decimation of the internal sites of a given cell, leading to renormalized quantities associated with the external sites. Defining the dimensionless couplings, $K_{ij} = \beta J_{ij}$ [$\beta = 1/(kT)$], the corresponding RG equations may be written in the general form [35,36],

$$K'_{\mu\nu} = \frac{1}{4} \ln\left(\frac{Z_{--}\, Z_{++}}{Z_{-+}\, Z_{+-}}\right), \tag{5}$$

where $Z_{S_\mu S_\nu}$ represent partition functions associated with the Hamiltonian $\mathcal{H}$ for a given unit cell with the external spins kept fixed ($S_\mu, S_\nu = \pm 1$),

$$Z_{S_\mu S_\nu} = \mathrm{Tr}_{\{S_i\ (i \neq \mu,\nu)\}} [\exp(-\beta \mathcal{H})]. \tag{6}$$

As usual in random magnetic models, the RG scheme is carried by following numerically the probability distribution $P(K_{ij})$ associated with the dimensionless couplings $\{K_{ij}\}$ [7]. Operationally, this probability distribution is represented by a pool of M real numbers (M is kept fixed throughout the whole RG procedure), from which one may compute its associated moments, at each renormalization step; in the limit $M \to \infty$ these moments should approach those of the distribution associated with $\{K_{ij}\}$. The process starts by creating M coupling constants $\{J_{ij}\}$ generated according to one of the distributions in Eqs. (2)–(4), yielding an initial pool of dimensionless couplings, $\{K_{ij}\} = \beta\{J_{ij}\}$, for a given temperature. An iteration consists in M operations, where in each of them one picks randomly a set of numbers from the pool (each number is assigned to a bond of a cell in Fig. 1) in order to generate the effective coupling according to Eq. (5), which will correspond to an element of the new pool. Following this procedure, one gets a new pool with the

same size M of the previous one, representing the renormalized probability distribution. During the RG procedure, the average, $\langle K_{ij}\rangle$, and the width, $\langle K_{ij}^2\rangle^{1/2}$, are of particular interest for the identification of the phases, in such a way that one may obtain the paramagnetic (**P**) and spin-glass (**SG**) phases, as dominated by the following attractors:

$$\begin{aligned} \langle K_{ij}\rangle &\to 0, \quad \left\langle K_{ij}^2\right\rangle^{1/2} \to 0, \qquad \textbf{P phase},\\ \langle K_{ij}\rangle &\to 0, \quad \left\langle K_{ij}^2\right\rangle^{1/2} \to \infty, \qquad \textbf{SG phase}. \end{aligned} \tag{7}$$

In fact, this procedure should be followed for many different initial pools of real numbers, over which one may compute sample averages. However, one may also get accurate critical-frontier estimates by analyzing a sufficiently large single pool; the results that follow were obtained by considering a single pool of size $M = 10^6$ real numbers.

Precisely at the **P**–**SG** phase transition, one starts with a given probability distribution $P(K_{ij})$ [e.g., constructed from one of the distributions in Eqs. (2)–(4)], and after a few RG iterations, one reaches the fixed-point distribution $P^*(K_{ij})$, which will not change in further RG steps. Strictly speaking, in order to approach such a distribution, one needs to be exactly at the critical temperature T_c associated with this transition. Operationally, for a given initial distribution, the associated critical temperature is estimated approximately, by following numerically $P(K_{ij})$, within the standard narrowing RG procedure (see, e.g., Refs. [7,35,36]). Herein, we have estimated T_c in most cases with a three-decimal-digit certainty (error bars on the fourth digit); therefore, we will deal with distributions that will be considered as "fixed-point" distributions for a certain number of RG iterations (typically around 10 iterations). At a given iteration step n, the corresponding distribution is obtained through a normalized histogram constructed from the pool of M dimensionless couplings $\{K_{ij}\}$, from which one computes its odd moments (which are all very small), as well as its even moments (which should remain essentially unchanged at the fixed point). A particular attention is given to its kurtosis κ and higher-order ratio of moments κ',

$$\kappa = \frac{\left\langle K_{ij}^4\right\rangle}{3\left\langle K_{ij}^2\right\rangle^2}, \quad \kappa' = \frac{\left\langle K_{ij}^6\right\rangle}{15\left\langle K_{ij}^2\right\rangle^3}, \tag{8}$$

which yield $\kappa = \kappa' = 1$, for a Gaussian distribution, whereas $\kappa,\kappa' > 1$ ($\kappa,\kappa' < 1$) for distributions with longer (shorter) tails, as compared with the Gaussian distribution.

Previous work on fixed-point distributions of Ising SGs on $D = 3$ MK hierarchical lattices verified that such distributions are close to a Gaussian; this conclusion was drawn essentially by analyzing their moments and kurtosis κ [7,11,27–29,47,48]. Moreover, it was shown that, for a given lattice, different initial distributions fall into a universal fixed-point distribution, after a few RG steps [29]. We present a detailed analysis of the functional form of this distribution for different hierarchical lattices.

Herein, we will examine several well-known distributions, as candidates for the universal fixed-point distribution of a given lattice. These distributions are expected to present some properties: (i) should be symmetric around the origin; (ii) particularly for the MK hierarchical lattices, they should converge to a Gaussian distribution for sufficiently large fractal dimensions [49]; (iii) in this latter case, it is desirable to search for distributions characterized by some tunable parameter such as to recover the Gaussian as a particular case. It should be mentioned that many distributions in the literature satisfy these requirements (see, e.g., Refs. [50–53]), although some of them are potentially most relevant, since they follow generalizations of the central limit theorem [50,51]. Below, we define the distributions that have provided the best fits for our data. First, we introduce the q-Gaussian distributions, characteristic of nonextensive statistical mechanics [50],

$$P(x) = \frac{\sqrt{\beta}}{A_q}[1-(1-q)\beta x^2]_+^{\frac{1}{1-q}}, \tag{9}$$

where $[u]_+ = u$, for $u > 0$ and zero otherwise, in such a way that they are characterized by a cutoff for $q < 1$. As usual, the quantity β is related to the width of the distribution, whereas A_q is a normalization factor that depends on the index q being given by [50,51]

$$A_q = \begin{cases} \frac{2\sqrt{\pi}}{(3-q)\sqrt{1-q}}\Gamma\left(\frac{1}{1-q}\right)\left[\Gamma\left(\frac{3-q}{2(1-q)}\right)\right]^{-1} & \text{if } q < 1,\\ \sqrt{\pi} & \text{if } q = 1,\\ \frac{\sqrt{\pi}}{\sqrt{q-1}}\Gamma\left(\frac{3-q}{2(q-1)}\right)\left[\Gamma\left(\frac{1}{q-1}\right)\right]^{-1} & \text{if } 1 < q < 3. \end{cases} \tag{10}$$

For $q < 1$ one gets distributions with a finite support, the Gaussian distribution is recovered as the particular case $q = 1$, whereas for $q > 1$ one has distributions with longer tails than those of the Gaussian. The distributions to be presented in the next section correspond to $\kappa > 1$ and, consequently, $q > 1$.

The second candidate for this purpose will be the stretched exponential,

$$P(x) = \frac{\lambda e^{-\lambda^\delta |x|^\delta}}{2\Gamma\left(1+\frac{1}{\delta}\right)} \quad (\delta > 0), \tag{11}$$

where the parameter λ is associated with the width of the distribution. Strictly speaking, the nomenclature "stretched exponential" applies for $0 < \delta < 1$, although for any $0 < \delta < 2$ one has distributions with longer tails than those of the Gaussian; the fits to be presented in the next section fall in this latter category.

The third proposal, to be called hereafter "stretched q-exponential" distribution, is given by

$$P(x) = \frac{\beta^{1/\gamma}}{B_{q,\gamma}}[1-(1-q)\beta|x|^\gamma]_+^{\frac{1}{1-q}}. \tag{12}$$

Considering $1 < q < 3$, the distribution above generalizes those defined in Eqs. (9) and (11), recovering such particular cases in the limits $\gamma \to 2$ and $q \to 1$ (taking $\gamma = \delta$ and $\beta = \lambda^\delta$), respectively. The normalization factor depends on both indices q and γ,

$$B_{q,\gamma} = \frac{2(q-1)^{-1/\gamma}\Gamma\left(1+\frac{1}{\gamma}\right)\Gamma\left(\frac{1}{q-1}-\frac{1}{\gamma}\right)}{\Gamma\left(\frac{1}{q-1}\right)}. \tag{13}$$

One should notice that besides the usual parameter related to the width of the distribution [β in Eqs. (9) and (12), and λ in Eq. (11)] one has one extra parameter in Eqs. (9) and (11), whereas in Eq. (12) one has two extra parameters, namely, q and γ. A compromise between the quality of the

fits and the number of parameters is certainly an important condition for choosing an appropriate fitting distribution. Other forms, like the Gaussian, Student's t, and α-stable Lévy distributions [52,53], were also considered for adjusting our data. In order to choose the best candidates for fixed-point distributions, we have investigated the quality of the fits through the standard χ^2 test, the agreement between the corresponding numerical data and distributions by means of different graphical representations, as well as by analyzing the quantities κ and κ' defined in Eq. (8). As it will be shown in the next section, the distributions defined in Eqs. (9)–(11) yielded the best fits for our numerical data.

III. RESULTS

The results that follow refer to the Ising SG model defined in the previous section, and in the case of the MK family [Fig. 1(a)] we have investigated different fractal dimensions varying in the interval from $D \approx 2.58$ (corresponding to unit cells with $p = 3$ parallel paths), up to $D = 7$ (corresponding to unit cells with $p = 64$ parallel paths), whereas in Fig. 1(b) one has a cell of the Wheatstone-Bridge family ($D \approx 3.58$), whose associated hierarchical lattice has been used in the literature to approximate models on the cubic lattice [20,35,36,38,54]. In order to approach appropriately fixed-point distributions, good estimates of the paramagnetic-SG critical temperatures are necessary in each case; except for the MK lattice with fractal dimension $D \approx 2.58$, we have computed critical temperatures T_c within a three-decimal-digit certainty, with the associated error bars on the fourth decimal digits. The estimates of T_c were carried by considering, in all cases, single pools of size $M = 10^6$ real numbers.

Flux diagrams representing the evolution of the probability distributions $P(K_{ij})$ under RG iterations, constructed from the coupling distributions in Eqs. (2)–(4), as well as from the q-Gaussian of Eq. (9) and stretched exponential of Eq. (11), are shown in Fig. 2 in terms of conveniently chosen variables [11,29], $\langle \tanh^2 K_{ij} \rangle$ versus $1/\langle K_{ij}^2 \rangle^{1/2}$ ($0 < \langle \tanh^2 K_{ij} \rangle < 1$ and $0 < 1/\langle K_{ij}^2 \rangle^{1/2} < \infty$), where the brackets $\langle\,\rangle$ denote averages over the corresponding distributions. One should call attention to the fact that the abscissa is related to the renormalized dimensionless temperature at each step of the RG process. In Fig. 2 the results for Ising SGs defined on two hierarchical lattices of the MK family [Fig. 1(a)] with different fractal dimensions, namely, $D = 3$ [Fig. 2(a)] and $D = 6$ [Fig. 2(b)], are presented. In both cases, throughout the evolution of the distributions one has the following. (i) The unstable fixed point, associated with the phase transition **P–SG** and assigned to the fixed-point distribution $P^*(K_{ij})$, is indicated by an arrow. (ii) The two attractors characterizing the corresponding phases are given by $\langle \tanh^2 K_{ij} \rangle \to 0$ and $1/\langle K_{ij}^2 \rangle^{1/2} \to \infty$ (**P** attractor), as well as $\langle \tanh^2 K_{ij} \rangle \to 1$ and $1/\langle K_{ij}^2 \rangle^{1/2} \to 0$ (**SG** attractor). (iii) These attractors define two basins of attraction, such that for initial distributions corresponding to values of $\langle \tanh^2 K_{ij} \rangle$ above (below) those of the fixed-point distribution, one is driven to the **SG** (**P**) attractor. (iv) From the five initial distributions considered, one sees that the q-Gaussian and stretched exponential appear both essentially as the fixed-point distribution, whereas the Gaussian comes as the third closest. In the representation of Fig. 2, the bimodal distribution corresponds the initial distribution that presents the "largest distance" with respect to the fixed-point distribution.

However, the most important outcome from Fig. 2 concerns the fact that all initial distributions, when considered at their corresponding critical temperatures T_c, approach a unique (i.e., universal) fixed-point distribution. The corresponding critical temperatures T_c are presented in Table I for Ising SGs on MK hierarchical lattices with several fractal dimensions D, as well as for the WB hierarchical lattice, for each initial distribution of couplings considered. Another important aspect in the

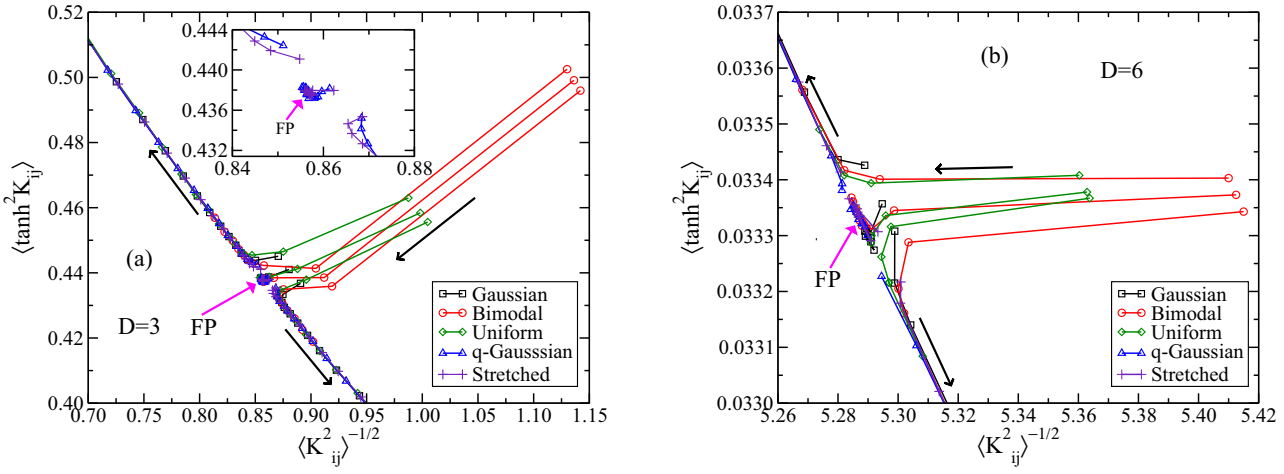

FIG. 2. (Color online) Flux diagrams of the probability distributions $P(K_{ij})$, constructed from the coupling distributions of Eqs. (2)–(4), as well as from the q-Gaussian of Eq. (9) and stretched exponential of Eq. (11), represented in suitable variables [11,29] for two hierarchical lattices of the Migdal-Kadanoff family [Fig. 1(a)] with fractal dimensions: (a) $D = 3$; (b) $D = 6$. In each case an arrow indicates the point associated with the fixed-point (FP) distribution $P^*(K_{ij})$; the region around this point is amplified in the inset of panel (a). In this representation one identifies clearly those initial distributions that differ most from the fixed-point distribution, as those that start the RG process with the "largest distance" from the latter (see, e.g., the evolution of the bimodal distribution). In the variables used, $\langle\rangle$ represent averages over the corresponding distributions.

TABLE I. Estimated values of q and β associated with the q-Gaussian distribution fit [cf. Eq. (9)], or equivalently, of λ and δ associated with the stretched-exponential fit [cf. Eq. (11)], when considered as fixed-point distributions for hierarchical lattices of the MK family with varying fractal dimensions $2.58 \leqslant D \leqslant 7$. In the case of the WB hierarchical lattice (fractal dimension $D \approx 3.58$) the best fit was obtained with the stretched-exponential distribution. The initial distributions (Gaussian, bimodal, and uniform) were considered at their corresponding critical values (kT_c/J); after a few iterations all distributions approached a fixed-point distribution as shown in Fig. 2, from which one may estimate the universal fixed-point critical temperature T_c^{FD}.

	D	q	β	λ	δ	kT_c/J (Gaussian)	kT_c/J (bimodal)	kT_c/J (uniform)	kT_c^{FD}/J
MK	2.58	1.08(2)	0.045(5)	0.21(2)	1.85(4)	0.291(5)	0.479(5)	0.201(5)	0.284(2)
MK	3.00	1.10(1)	0.43(3)	0.66(2)	1.76(5)	0.8797(5)	1.1362(5)	0.5762(5)	0.856(1)
MK	3.58	1.11(1)	1.4(1)	1.19(2)	1.74(5)	1.5718(5)	1.8219(5)	0.9825(5)	1.539(1)
MK	4.00	1.11(1)	2.5(2)	1.59(2)	1.75(5)	2.0808(5)	2.3067(5)	1.2716(5)	2.046(2)
MK	4.58	1.09(2)	4.8(3)	2.16(3)	1.80(5)	2.8623(5)	3.0522(5)	1.7147(5)	2.838(2)
MK	5.00	1.08(2)	6.8(2)	2.60(3)	1.83(5)	3.4799(5)	3.6522(5)	2.0662(5)	3.464(2)
MK	6.00	1.05(2)	15.1(2)	3.87(4)	1.90(4)	5.2908(5)	5.4125(5)	3.0955(5)	5.289(3)
MK	7.00	1.03(1)	31.3(1)	5.58(4)	1.95(3)	7.7402(5)	7.8273(5)	4.4957(5)	745(6)
WB	3.58			0.78(2)	1.57(3)	0.9821(5)	1.1166(5)	0.6122(5)	0.948(2)

representation of Fig. 2 concerns the fact that one may compute the coordinates associated with $P^*(K_{ij})$, leading to critical-temperature estimates related with each fixed-point distribution. Herein, we define this temperature as $(kT_c^{FD}/J) \equiv \langle (K_{ij}^*)^2 \rangle^{-1/2}$, to be computed for $P(K_{ij}) = P^*(K_{ij})$. For the cases exhibited in Fig. 2 one has $(kT_c^{FD}/J) = 0.856(1)$ $(D = 3)$ and $(kT_c^{FD}/J) = 5.289(3)$ $(D = 6)$, respectively. It should be mentioned that T_c^{FD} is defined only for hierarchical lattices, being associated with fixed-point distributions within the RG approach, having no physical counterpart on Bravais lattices.

In Fig. 3 we present data of the fixed-point distribution for the Ising SG on a MK hierarchical lattice with fractal dimension $D = 3$, together with the two best fits found. The Gaussian distribution of Eq. (2) was considered as the initial distribution for the couplings, at its corresponding critical temperature, $(kT_c/J) = 0.8797(5)$ (cf. Table I). Data for a wide range of RG iterations, from $n = 4$ up to $n = 16$, are exhibited. In the linear representation of Fig. 3(a), both q-Gaussian and stretched exponential appear to yield equally good fits. However, in the corresponding inset one sees that in a representation $\ln_q P(K_{ij})$ versus $K_{ij}^2[\ln_q u = (u^{1-q} - 1)/(1-q)]$ [50], the q-Gaussian $[q = 1.10(1)]$ yields a straight line, producing a good fit for both central region and tails of the distribution, appearing to be slightly better than the one produced by the stretched exponential [with $\delta = 1.76(5)$]. In Fig. 3(b) the same data is exhibited in a log-linear representation, where due to the wide spread of the data in the tails, in the inset we have also considered histograms with larger bins, i.e., increased by a factor of 2 for $2 \leqslant |K_{ij}| \leqslant 4$, and by a factor of 4 in the range $|K_{ij}| > 4$. From this later representation, both q-Gaussian and stretched exponential distributions yielded equally good fits;

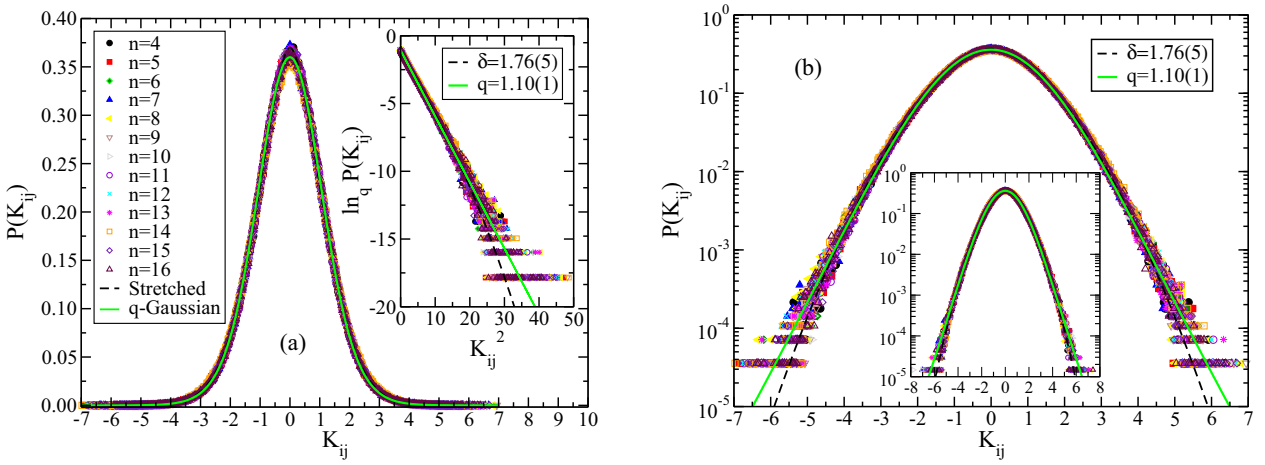

FIG. 3. (Color online) Data of the fixed-point distribution for the Ising SG on a MK hierarchical lattice with $D = 3$. For all data shown, the Gaussian distribution of Eq. (2) was considered as initial distribution, at its associated critical temperature (cf. Table I). For a large range of RG iterations, from $n = 4$ up to $n = 16$ (denoted by different symbols), one gets typically a fixed-point distribution. (a) In the linear representation, both q-Gaussian [with $q = 1.10(1)$] and stretched [with $\delta = 1.76(5)$] fits are indiscernible. In the inset we represent the same data as $\ln_q P(K_{ij})$ vs K_{ij}^2, where the q-Gaussian fit (full green line) follows a straight line, being compared with the stretched-exponential one (dashed black line). (b) The same data of (a) is exhibited in a log-linear representation, where the q-Gaussian (full green line) and stretched exponential (dashed black line) fits are shown. In the inset we represent the same data by considering larger bins for the histograms (see text).

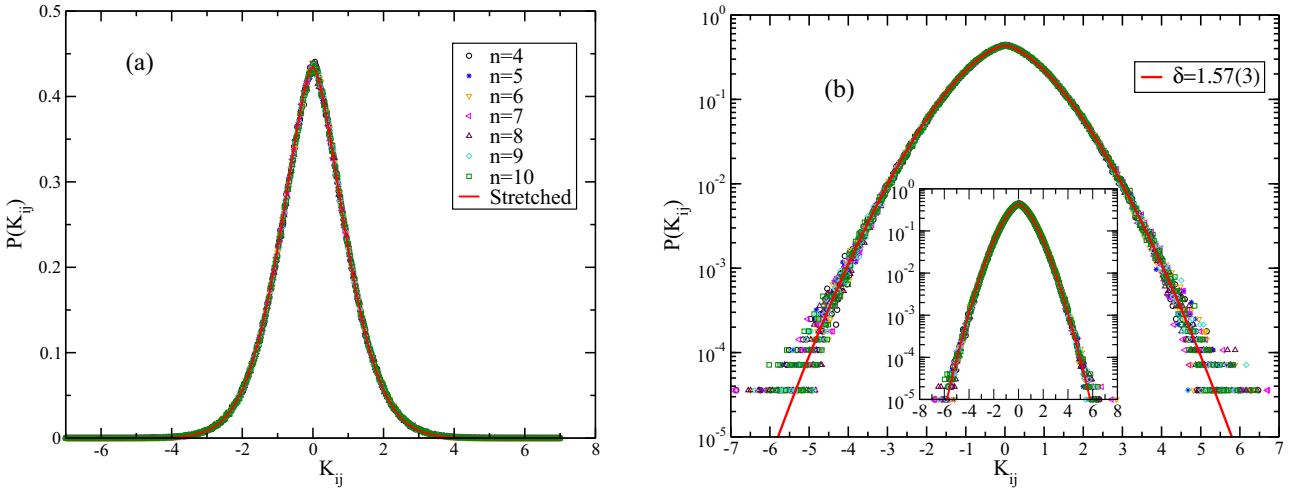

FIG. 4. (Color online) Data of the fixed-point distribution for the Ising SG on a WB hierarchical lattice with $D \approx 3.58$. The Gaussian distribution of Eq. (2) was considered as initial distribution, at its associated critical temperature (cf. Table I). For a given range of RG iterations, from $n = 4$ up to $n = 10$ (denoted by different symbols), one gets typically a fixed-point distribution. (a) In the linear representation, the stretched exponential of Eq. (11) [with $\delta = 1.57(3)$] is presented. (b) The same data of (a) is exhibited in a log-linear representation; in the inset we represent the same data by considering larger bins for the histograms (see text).

this conclusion is reinforced by the χ^2 test analysis, as well as by the quantities κ and κ' defined in Eq. (8), which gave typically values of the same order of magnitude.

A similar investigation was carried for the WB hierarchical lattice defined by the unit cell of Fig. 1(b). Together with the data, the best fit found is shown in Fig. 4, namely, the stretched exponential of Eq. (11) [with $\delta = 1.57(3)$, represented by the full red line]. Both data and fitting distribution are exhibited in the linear-linear representation [Fig. 4(a)] and a log-linear representation [Fig. 4(b)]. In the latter case, due to the wide spread of the data in the tails, we present the histogram obtained by enlarging the size of bins in the inset of Fig. 4(b): bins were increased by a factor of 2 for $2 \leqslant |K_{ij}| \leqslant 4$, and by a factor of 4 in the range $|K_{ij}| > 4$. These results show the robustness of the stretched-exponential distribution in this fitting.

For all hierarchical lattices of the MK family investigated herein we have found that both q-Gaussian and stretched-exponential distributions yielded equally good fits. These conclusions were reached by plotting the data in different representations (as shown in Fig. 3 for the case $D = 3$), by applying the χ^2 test, as well as by investigating the quantities κ and κ' defined in Eq. (8); in all analyses carried out, these two distributions were essentially equally acceptable. In each case, the initial distributions (Gaussian, bimodal, and uniform) were considered at their corresponding critical temperatures T_c, and after a few RG iterations (typically four iterations), the renormalized distributions approached the fixed-point distribution. The estimated values of q and β associated with the q-Gaussian distribution fit [cf. Eq. (9)], or equivalently, of λ and δ associated with the stretched-exponential fit [cf. Eq. (11)], are given in Table I. In this table we also present T_c for each initial distribution considered, as well as T_c^{FD}, for hierarchical lattices of the MK family with several dimensions. The universal fixed-point critical temperatures T_c^{FD} were calculated through flux diagrams similar to those exhibited in Fig. 2, as described above. The parameters q and β, associated with the q-Gaussian distribution fit of Eq. (9), were computed at each RG step along which the distribution remained essentially unchanged (e.g., from $n = 4$ up to $n = 16$ in the case of Fig. 3) by using the Marquardt-Levenberg algorithm (see Ref. [55] for a description of the method), with a similar procedure for the parameters λ and δ of the stretched-exponential distribution. The estimates (including error bars) for q and β (as well as for λ and δ) presented in Table I correspond to an analysis over these RG iterations.

In Table I we also present the estimated values of λ and δ, corresponding to the stretched-exponential fit, when considered as fixed-point distribution for the WB hierarchical lattice, as shown in Fig. 4. Similar to the procedure used for the MK cases, the parameters of the corresponding distribution were calculated for a given range of RG iterations, from $n = 4$ up to $n = 10$, where one gets typically a fixed-point distribution. It should be mentioned that the stretched q-exponential fit [cf. Eq. (12)] was also analyzed as a potential candidate for this case; however, we verified that this distribution was not robust by increasing the size of the bins in a log-linear representation [cf., e.g., Figs. 3(b) and 4(b)]. In fact, we found that $q \to 1$, as the bins were gradually increased, so that the stretched-exponential fit was recovered in this limit.

Analyzing the results of Table I, one notices a gradual decrease in the value of q for MK lattices with sufficiently large fractal dimensions (e.g., $D > 4$), suggesting that when the number of parallel paths of the unit cell goes to infinity, one should approach the limit $q \to 1$, indicating that the fixed-point distribution converges to a Gaussian, as predicted in Ref. [49]. A similar behavior may be seen with respect to the parameter δ in the stretched-exponential fit, which for $3 \leqslant D \leqslant 7$ increases slowly towards the limit $\delta \to 2$, showing the convergence to the Gaussian fixed-point distribution.

Another interesting aspect from Table I concerns the fact that the critical-temperature estimates of the WB hierarchical lattice are much closer to those of the MK lattice with $D = 3$ than to the ones of a MK lattice with the same fractal

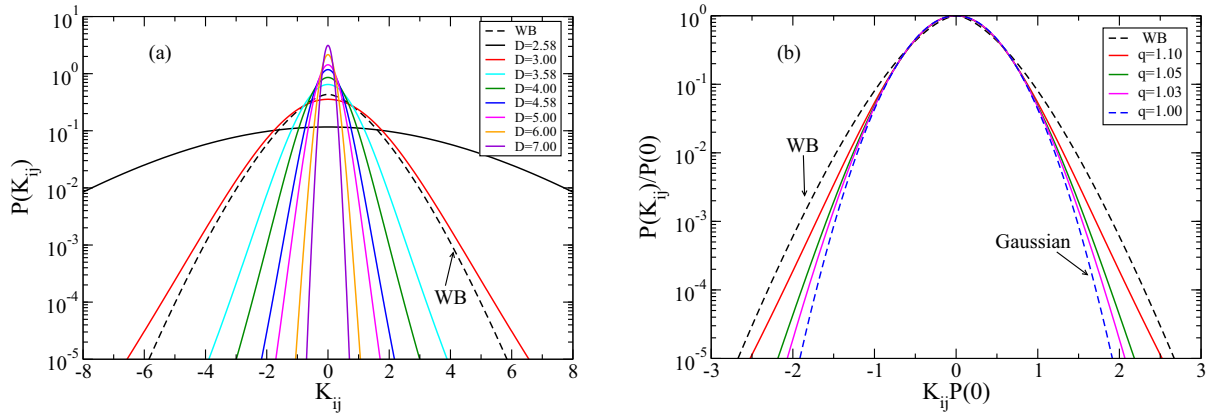

FIG. 5. (Color online) Fixed-point distributions for the hierarchical lattices of the MK family with several fractal dimensions in the range $2.58 \leqslant D \leqslant 7$, following the q-Gaussian distribution fit of Eq. (9), are represented as full lines, whereas the one for the WB hierarchical lattice that follows the stretched-exponential fit [cf. Eq. (11)] is represented by a dashed black line. (a) In a log-linear representation, where one sees that the widths of these distributions decrease for increasing fractal dimensions (a similar behavior occurs if one considers the stretched-exponential fits from Table I). (b) In the variables used, those q-Gaussian distributions with the same index q do not depend on their width, and collapse into a single curve: consequently, the full red line (outer full line) applies to those hierarchical lattices of the MK family with fractal dimensions in the range $2.58 \leqslant D \leqslant 5$, for which $q = 1.10$ within the error bars (cf. Table I); the full lines correspond to decreasing values of q from outer to inner. The dashed blue line in panel (b) corresponds to the Gaussian distribution.

dimension, namely, $D \approx 3.58$. This reflects the fact that the WB hierarchical lattice should be considered as an approach to the cubic lattice, as discussed in Ref. [20]. Indeed, the critical-temperature estimates $(kT_c/J) = 0.9821(5)$ (Gaussian distribution) and $(kT_c/J) = 1.1166(5)$ (bimodal distribution) of Table I are in very good agreement with those from Monte Carlo simulations on a cubic lattice; for the first case, one should mention the result $(kT_c/J) = 0.951(9)$ [14], from which our value keeps a relative discrepancy of about 3%. The most striking outcome concerns the one for the critical temperature in the case of a bimodal distribution, which lies in between the two estimates, $(kT_c/J) = 1.120(4)$ [14] and $(kT_c/J) = 1.1019(29)$ [19], where the latter appeared recently from an extensive numerical investigation. However, the corresponding estimates of the MK lattice with $D = 4$, namely, $(kT_c/J) = 2.0808(5)$ (Gaussian distribution) and $(kT_c/J) = 2.3067(5)$ (bimodal distribution), when compared with those of Monte Carlo simulations on a four-dimensional hypercubic lattice, $(kT_c/J) \approx 1.80$ [56] and $(kT_c/J) = 2.00(4)$ [57], lead to relative discrepancies around 13%.

In Fig. 5 we exhibit the q-Gaussian distributions of Eq. (9), as well as the stretched-exponential fit of Eq. (11), considered as fixed-point distributions for the hierarchical lattices of the MK family (full lines), and for the WB hierarchical lattice (dashed black line), respectively. From Fig. 5(a) one sees that the q-Gaussian distributions of the MK family decrease their width for increasing values of D, signaling an increase in the corresponding critical temperatures with D; it should be mentioned that a similar behavior occurs if one considers the stretched-exponential fits specified in Table I. Moreover, one sees clearly that the WB fixed-point distribution is much closer to the one of the MK lattice with $D = 3$ than to the one with fractal dimension $D \approx 3.58$ of the same lattice, reinforcing the argument that the WB hierarchical lattice should be considered as an approach to the cubic lattice [20]. The representation used in Fig. 5(b) is very convenient for q-Gaussian distributions, since these distributions become independent of their widths, depending only on the index q. Therefore, since all hierarchical lattices of the MK family in the range $2.58 \leqslant D \leqslant 5$ studied herein presented $q = 1.10$, within the error bars (cf. Table I), they have collapsed into a single curve in Fig. 5(b) (full red line). Furthermore, from Fig. 5(b) one sees that the distributions for larger fractal dimensions, namely, $D = 6$ (represented by the curve for $q = 1.05$) and $D = 7$ (represented by the curve for $q = 1.03$), present a clear tendency towards the Gaussian limit (dashed blue line).

From the fixed-point distribution $P^*(K_{ij})$ one can calculate numerically the exponent ν associated with the divergence of the correlation length at the phase transition [7,58,59]. For that, in each case one considers two temperatures T_1 and T_2, slightly below T_c^{FD} (see Table I), such that $T_2 < T_1 < T_c^{FD}$. Since the estimates of T_c^{FD} in Table I were done up to three decimal digits, we have defined $[(kT_1)/J] = [(kT_c^{FD})/J] - 10^{-3}$, whereas $T_2 = T_1 - \delta T$, with δT representing a small temperature variation. Then, one follows the RG procedure described in the previous section, starting with these two temperatures, so that at a given RG step n one has the respective widths $\langle K_{ij}^2 \rangle_{1,n}^{1/2}$ (RG scheme starting at temperature T_1) and $\langle K_{ij}^2 \rangle_{2,n}^{1/2}$ (RG scheme starting at temperature T_2); since $T_2 < T_1$, one has that $\langle K_{ij}^2 \rangle_{2,n}^{1/2} > \langle K_{ij}^2 \rangle_{1,n}^{1/2}$, for every step n. Hence the exponent ν_n at a step n is defined as

$$\nu_n = \frac{\ln 2}{\ln(\Delta_{n+1}/\Delta_n)}, \quad \Delta_n = \langle K_{ij}^2 \rangle_{2,n}^{1/2} - \langle K_{ij}^2 \rangle_{1,n}^{1/2}. \qquad (14)$$

If one considers δT sufficiently small, the estimates ν_n fluctuate around a given value for a certain range of RG iterations. In the present analysis we have considered the q-Gaussian distribution of Eq. (9) as initial distributions in the case of the MK hierarchical lattices [using the stretched exponential of Eq. (11) as initial distributions yielded similar

TABLE II. Estimates for the exponent ν, considering the q-Gaussian distribution of Eq. (9) as initial distributions in the case of the MK hierarchical lattices, whereas for the WB lattice we have used the stretched exponential of Eq. (11) as initial distribution.

	MK								WB
D	2.58	3.00	3.58	4.00	4.58	5.00	6.00	7.00	3.58
ν	13.1(9)	2.97(5)	1.77(9)	1.49(9)	1.29(4)	1.20(6)	1.08(5)	1.04(3)	3.02(7)

results, within the error bars], whereas for the WB lattice, we have analyzed the stretched exponential of Eq. (11) as initial distribution. Considering $[k(\delta T)/J] = 10^{-6}$, ν_n remained stable (i.e., presenting small fluctuations around a given mean value), for a certain range of RG iterations (typically 10 RG iterations); the results for the exponent ν presented in Table II correspond to averages over these iterations.

The estimates in Table II regarding MK lattices with fractal dimensions $D = 3$, 4, 5, and 6 essentially coincide with those already computed in Ref. [59]. In what concerns the WB lattice, we obtained $\nu = 3.02(7)$. One should notice that the estimates for the MK lattice with $D = 3$ and WB lattice agree within the error bars, yielding $\nu \approx 3.0$. Moreover, our value for the WB lattice also agrees with the recent one on the same lattice, $\nu = 3.25(66)$ [54], although both represent overestimates with respect to results from Monte Carlo simulations on a cubic lattice, which by considering different probability distributions for the couplings, yielded typically a universal value, $\nu \approx 2.5$ [14,17–19]. It should be mentioned that the values given in Table II represent universal exponents for each hierarchical lattice considered, since they were obtained from universal fixed-point distributions; in this sense, our estimate for the WB lattice presents a relative discrepancy of about 15% with respect to the most recent result from extensive numerical simulations, $\nu = 2.562(42)$ [19]. The discrepancy increases further when comparing the result of the $D = 4$ MK hierarchical lattice, $\nu = 1.49(9)$, with the one from Monte Carlo simulations on a four-dimensional hypercubic lattice, $\nu = 1.025(15)$ [56]. It is possible that such significant discrepancies may be associated with the linearization procedure used to obtain Eq. (14), as argued in Ref. [60].

In Fig. 6 we present data of the fixed-point distributions in a log-linear representation for the cases of the MK hierarchical lattice with $D = 3$ [Fig. 6(a)] and the WB hierarchical lattice [Fig. 6(b)]. In each case, besides the fitting distributions used in Figs. 3(b) and 4(b), respectively, we also show fits from three other distributions, namely, the Gaussian, Student's t, and α-stable Lévy distributions [52,53]; in the WB case, we considered the stretched q-exponential fit of Eq. (12) as well. In the Student's t fits, the number of degrees of freedom (by definition a positive integer) considered for the best fit was $m = 19$ [for both Figs. 6(a) and 6(b)], whereas for those of the α-stable Lévy we have used $\alpha = 1.98(1)$ in Fig. 6(a) and $\alpha = 1.95(2)$ in Fig. 6(b). Ones sees clearly that these three attempts, namely, Gaussian, Student's t, and α-stable Lévy distributions all fail in some way to fit the data appropriately, either in the tails, or in the central region, as shown in the insets. A curious situation occurs in Fig. 6(b), where the stretched q-exponential fit is presented, showing apparently a good agreement with the data. In fact, as mentioned before, we verified that this distribution was not robust by increasing the size of the bins in the tails, so that $q \to 1$ as the bins were gradually increased, recovering the stretched-exponential fit in this limit [see Fig. 4(b)]. Hence, in the present approach, the

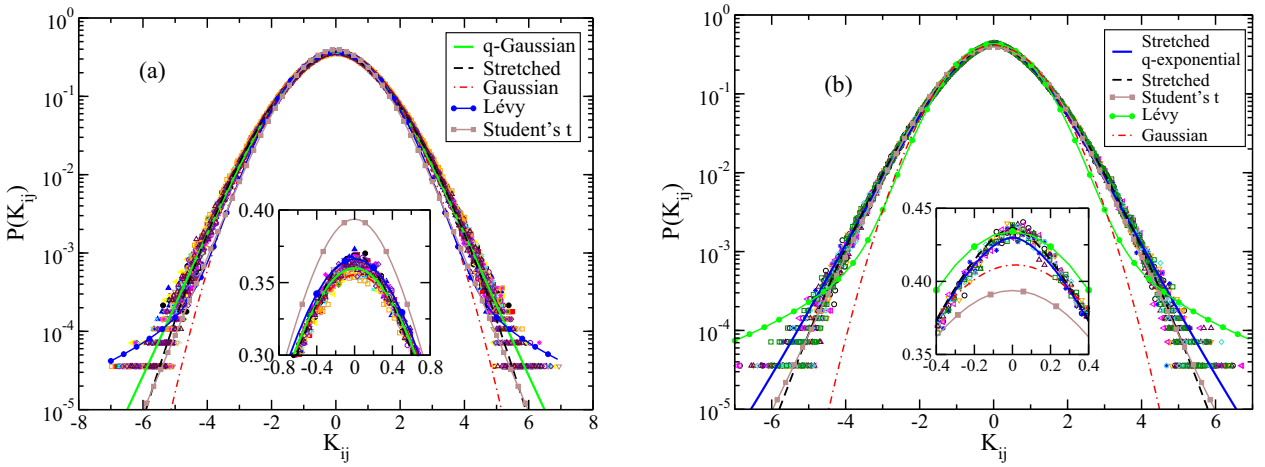

FIG. 6. (Color online) Data of fixed-point distributions are represented in a log-linear representation. (a) Ising SG on a MK hierarchical lattice with $D = 3$; apart from the distributions used in Fig. 3(b) (stretched exponential and q-Gaussian), the Gaussian, α-stable Lévy, and Student's t distributions were also considered for fitting the data. (b) Ising SG on a WB hierarchical lattice with $D \approx 3.58$; apart from the stretched-exponential distribution used in Fig. 4(b), the Gaussian, α-stable Lévy, Student's t, and stretched q-exponential [cf. Eq. (12)] distributions were also considered for fitting the data. The central region of the plots are amplified (linear-linear scale) in the respective insets.

q-Gaussian and stretched-exponential distributions appeared as equally acceptable good fits for the MK lattice, whereas for the WB lattice, the stretched exponential yielded the best fit for the fixed-point distribution.

IV. CONCLUSIONS

We have investigated numerically the fixed-point distributions for the couplings of nearest-neighbor-interacting Ising spin glasses on hierarchical lattices. Hierarchical lattices belonging to the Migdal-Kadanoff family with fractal dimensions in the range $2.58 \leqslant D \leqslant 7$, as well as a lattice of the Wheatstone-Bridge family with fractal dimension $D \approx 3.58$ were considered. Three initial distributions for the couplings were analyzed, namely, the Gaussian, bimodal, and uniform ones. In all cases considered, after a few iterations of the renormalization-group procedure (typically four iterations), the associated probability distributions approached fixed universal shapes.

For the Migdal-Kadanoff lattices, the fixed-point distributions were shown to be well fitted either by stretched exponentials, or by q-Gaussian distributions; both fittings recover the expected Gaussian limit as $D \to \infty$. For the q-Gaussian fits we have found $q \approx 1.10$, for $2.58 \leqslant D \leqslant 5$, whereas for $D = 6$ and 7 we have noticed a slow decrease in the value of q towards the limit $q \to 1$. Moreover, in the case of the Wheatstone-Bridge lattice, the fixed distribution was shown to be well fitted by a stretched exponential. Hence, if one considers the stretched-exponential distribution, $P(x) \sim \exp(-\lambda^{\delta}|x|^{\delta})$, as the appropriate fixed-point distribution for both lattices studied, one has δ typically varying in the range $\delta \in [1.75, 1.95]$, for MK lattices with fractal dimensions $2.58 \leqslant D \leqslant 7$, whereas in the WB lattice, $\delta \approx 1.57$, representing a distribution more "different" from the Gaussian, than those found for the Ising spin glasses on the lattices of the Migdal-Kadanoff family.

The knowledge of the functional form of fixed-point distributions represents a relevant question for spin-glass models on hierarchical lattices. From these distributions one may compute important critical quantities, like universal critical exponents, which in the case of Ising spin glasses should be independent of the initial distribution of couplings considered. The universality of critical exponents has been found in most recent numerical simulations of spin-glass models on Bravais lattices, in agreement with the present investigation. In this work, we have presented a proposal for the functional forms of fixed-point distributions on some hierarchical lattices, which yielded quite good agreements with the numerical data. These distributions are expected to contribute to a better understanding of short-range Ising spin glasses on Bravais lattices.

ACKNOWLEDGMENTS

The partial financial support from CNPq and FAPERJ (Brazilian funding agencies) is acknowledged.

[1] V. Dotsenko, *Introduction to the Replica Theory of Disordered Statistical Systems* (Cambridge University Press, Cambridge, UK, 2001).

[2] H. Nishimori, *Statistical Physics of Spin Glasses and Information Processing* (Oxford University Press, Oxford, 2001).

[3] C. de Dominicis and I. Giardina, *Random Fields and Spin Glasses – A Field Theory Approach* (Cambridge University Press, Cambridge, UK, 2006).

[4] E. Marinari, G. Parisi, and J. J. Ruiz-Lorenzo, in *Spin Glasses and Random Fields*, edited by A. P. Young (World Scientific, Singapore, 1998), pp. 59.

[5] T. Castellani and A. Cavagna, Spin-glass theory for pedestrians, J. Stat. Mech. (2005) P05012.

[6] G. Parisi, Spin glasses and fragile glasses: Statics, dynamics, and complexity, Proc. Natl. Acad. Sci. U.S.A. **103**, 7948 (2006).

[7] B. W. Southern and A. P. Young, Real space rescaling study of spin glass behavior in three dimensions, J. Phys. C **10**, 2179 (1977).

[8] R. N. Bhatt and A. P. Young, Search for a Transition in the Three-dimensional ±J Ising Spin-glass, Phys. Rev. Lett. **54**, 924 (1985).

[9] A. T. Ogielski and I. Morgenstern, Critical Behavior of Three-dimensional Ising Spin-glass Model, Phys. Rev. Lett. **54**, 928 (1985).

[10] A. J. Bray and M. A. Moore, in *Heidelberg Colloquium on Glassy Dynamics*, edited by J. L. van Hemmen and I. Morgenstern, Lecture Notes in Physics Vol. 275 (Springer-Verlag, Berlin, 1987), pp. 121.

[11] E. M. F. Curado and J. L. Meunier, Spin-glass in low dimensions and the Migdal-Kadanoff approximation, Physica A **149**, 164 (1988).

[12] R. N. Bhatt and A. P. Young, Numerical studies of Ising spin glasses in two, three, and four dimensions, Phys. Rev. B **37**, 5606 (1988).

[13] A. P. Young and H. G. Katzgraber, Absence of an Almeida-Thouless Line in Three-dimensional Spin Glasses, Phys. Rev. Lett. **93**, 207203 (2004).

[14] H. G. Katzgraber, M. Körner, and A. P. Young, Universality in three-dimensional Ising spin glasses: A Monte Carlo study, Phys. Rev. B **73**, 224432 (2006).

[15] T. Jörg, H. G. Katzgraber, and F. Krząkala, Behavior of Ising spin glasses in a magnetic field, Phys. Rev. Lett. **100**, 197202 (2008).

[16] T. Jörg and H. G. Katzgraber, Evidence for universal scaling in the spin-glass phase, Phys. Rev. Lett. **101**, 197205 (2008).

[17] M. Hasenbusch, A. Pelissetto, and E. Vicari, The critical behavior of 3D Ising spin glass models: Universality and scaling corrections, J. Stat. Mech. (2008) L02001.

[18] M. Hasenbusch, A. Pelissetto, and E. Vicari, Critical behavior of three-dimensional Ising spin glass models, Phys. Rev. B **78**, 214205 (2008).

[19] M. Baity-Jesi *et al.*, Critical parameters of the three-dimensional Ising spin glass, Phys. Rev. B **88**, 224416 (2013).

[20] C. Tsallis and A. C. N. de Magalhães, Pure and random Potts-like models: Real-space renormalization-group approach, Phys. Rep. **268**, 305 (1996).

[21] A. A. Migdal, Phase transitions in gauge and spin-lattice systems, Sov. Phys. JETP **42**, 743 (1976).
[22] L. P. Kadanoff, Notes on Migdal's recursion formulas, Ann. Phys. (N.Y.) **100**, 359 (1976).
[23] P. M. Chaikin and T. C. Lubensky, *Principles of Condensed Matter Physics* (Cambridge University Press, Cambridge, UK, 1995).
[24] M. Nifle and H. J. Hilhorst, New Critical-point exponent and new scaling laws for short-range Ising spin glasses, Phys. Rev. Lett. **68**, 2992 (1992).
[25] F. D. Nobre, Real-space renormalization-group approaches for two-dimensional Gaussian Ising spin glass, Phys. Lett. A **250**, 163 (1998).
[26] M. A. Moore, H. Bokil, and B. Drossel, Evidence for the droplet picture of spin glasses, Phys. Rev. Lett. **81**, 4252 (1998).
[27] E. Nogueira, Jr., S. Coutinho, F. D. Nobre, E. M. F. Curado, and J. R. L. de Almeida, Short-range Ising spin glass: Multifractal properties, Phys. Rev. E **55**, 3934 (1997).
[28] E. Nogueira, Jr., S. Coutinho, F. D. Nobre, and E. M. F. Curado, Short-range Ising spin glasses: A critical exponent study, Physica A **257**, 365 (1998).
[29] E. Nogueira, Jr., S. Coutinho, F. D. Nobre, and E. M. F. Curado, Universality in short-range Ising spin glasses, Physica A **271**, 125 (1999).
[30] E. M. F. Curado, F. D. Nobre, and S. Coutinho, Ground-state degeneracies of Ising spin glasses on diamond hierarchical lattices, Phys. Rev. E **60**, 3761 (1999).
[31] F. D. Nobre, On the universal behavior of two-dimensional Ising spin glasses, Physica A **280**, 456 (2000).
[32] B. Drossel, H. Bokil, M. A. Moore, and A. J. Bray, The link overlap and finite size effects for the 3D Ising spin glass, Eur. Phys. J. B **13**, 369 (2000).
[33] F. D. Nobre, Phase diagram of the two-dimensional ±J Ising spin glass, Phys. Rev. E **64**, 046108 (2001).
[34] F. D. Nobre, The two-dimensional ±J Ising spin glass: A model at its lower critical dimension, Physica A **319**, 362 (2003).
[35] O. R. Salmon and F. D. Nobre, Spin-glass attractor on tridimensional hierarchical lattices in the presence of an external magnetic field, Phys. Rev. E **79**, 051122 (2009).
[36] O. R. Salmon, B. T. Agostini, and F. D. Nobre, Ising spin glasses on Wheatstone–Bridge hierarchical lattices, Phys. Lett. A **374**, 1631 (2010).
[37] T. Jörg and F. Krząkala, The nature of the different zero-temperature phases in discrete two-dimensional spin glasses: Entropy, universality, chaos and cascades in the renormalization group flow, J. Stat. Mech. (2012) L01001.
[38] S. T. O. Almeida, E. M. F. Curado, and F. D. Nobre, Chaos and stiffness exponents for short-range Gaussian Ising spin glasses, J. Stat. Mech. (2013) P06013.
[39] W. L. McMillan, Domain-wall renormalization-group study of the two-dimensional random Ising model, Phys. Rev. B **29**, 4026 (1984).
[40] W. L. McMillan, Domain-wall renormalization-group study of the three-dimensional random Ising model, Phys. Rev. B **30**, 476 (1984).
[41] A. J. Bray and M. A. Moore, Lower critical dimension of Ising spin glasses: A numerical study, J. Phys. C **17**, L463 (1984).
[42] W. L. McMillan, Domain-wall renormalization-group study of the three-dimensional random Ising model at finite temperature, Phys. Rev. B **31**, 340 (1985).
[43] A. K. Hartmann, Scaling of stiffness energy for three-dimensional ±J Ising spin glasses, Phys. Rev. E **59**, 84 (1999).
[44] A. K. Hartmann and A. P. Young, Lower critical dimension of Ising spin glasses, Phys. Rev. B **64**, 180404 (2001).
[45] S. Boettcher, Stiffness of the Edwards-Anderson Model in all dimensions, Phys. Rev. Lett. **95**, 197205 (2005).
[46] A. K. Hartmann, A. J. Bray, A. C. Carter, M. A. Moore, and A. P. Young, Stiffness exponent of two-dimensional Ising spin glasses for nonperiodic boundary conditions using aspect-ratio scaling, Phys. Rev. B **66**, 224401 (2002).
[47] S. Prakash and I. A. Campbell, Studies of the Migdal-Kadanoff renormalization group for Ising systems, Physica A **235**, 507 (1997).
[48] O. D. da Silva-Neto, D. Sc. thesis, Universidade Federal de Pernambuco, 1999.
[49] E. Gardner, A spin glass model on a hierarchical lattice, J. Phys. (Paris) **45**, 1755 (1984).
[50] C. Tsallis, *Introduction to Nonextensive Statistical Mechanics - Approaching a Complex World* (Springer, New York, 2009).
[51] C. Tsallis, S. V. F. Levy, A. M. C. Souza, and R. Maynard, Statistical-mechanical Foundation of the Ubiquity of Lévy Distributions in Nature, Phys. Rev. Lett. **75**, 3589 (1995).
[52] V. Krishnan, *Probability and Random Processes* (John Wiley and Sons, Inc., Hoboken, NJ, 2006).
[53] K. Jacobs, *Stochastic Processes for Physicists* (Cambridge University Press, Cambridge, UK, 2010).
[54] F. Antenucci, A. Crisanti and L. Leuzzi, Critical study of hierarchical lattice renormalization group in magnetic ordered and quenched disordered systems: Ising and Blume-Emery-Griffiths models, J. Stat. Phys. **155**, 909 (2014).
[55] J. J. Moré, in *Numerical Analysis*, edited by G. A. Watson, Lecture Notes in Mathematics Vol. 630 (Springer-Verlag, Berlin, 1978), pp. 105.
[56] T. Jörg and H. G. Katzgraber, Universality and universal finite-size scaling functions in four-dimensional Ising spin glasses, Phys. Rev. B **77**, 214426 (2008).
[57] K. Hukushima, Domain-wall free energy of spin-glass models: Numerical method and boundary conditions, Phys. Rev. E **60**, 3606 (1999).
[58] J. Machta and M. S. Cao, Differential Migdal-Kadanoff renormalization group for disordered systems, J. Phys. A **25**, 529 (1992).
[59] R. S. Júnior and F. D. Nobre, A Migdal-Kadanoff renormalization-group approach for the XY spin glass, Z. Phys. B **101**, 455 (1996).
[60] J. R. L. de Almeida, Perturbation study of the linear renormalization group for spin glasses, J. Phys. A **26**, 193 (1993).